Cholesterol Slows down the Lateral Mobility of an Oxidized Phospholipid in a Supported Lipid Bilayer

Birgit Plochberger,[†,#] Thomas Stockner,[‡,§,#] Salvatore Chiantia,[||] Mario Brameshuber,[†] Julian Weghuber,[†] Albin Hermetter,[⊥] Petra Schwille,[||] and Gerhard J. Schütz*,[†]

[†]*Biophysics Institute, Johannes Kepler University Linz, A-4040 Linz, Austria,* [‡]*Bioresources, Austrian Institute of Technology, Seibersdorf, A-2444, Austria,* [§]*Department of Medical Chemistry, Medical University of Vienna, A-1090 Vienna, Austria,* [||]*Technical University of Dresden, Biotechnologisches Zentrum, Dresden, Germany, and* [⊥]*Institute of Biochemistry, Graz University of Technology, A-8010 Graz, Austria.* [#]*Authors contributed equally to this work.*

We investigated the mobility and phase-partitioning of the fluorescent oxidized phospholipid analogue 1-palmitoyl-2-glutaroyl-*sn*-glycero-3-phospho-*N*-Alexa647-ethanolamine (PGPE-Alexa647) in supported lipid bilayers. Compared to the conventional phospholipid dihexadecanoylphosphoethanolamine (DHPE)-Bodipy we found consistently higher diffusion constants. The effect became dramatic when immobile obstacles were inserted into the bilayer, which essentially blocked the diffusion of DHPE-Bodipy but hardly influenced the movements of PGPE-Alexa647. In a supported lipid bilayer made of 1,2-dioleoyl-*sn*-glycero-3-phosphocholine (DOPC), the differences in probe mobility leveled off with increasing cholesterol content. Using coarse-grained molecular dynamics simulations, we could ascribe this effect to increased interactions between the oxidized phospholipid and the membrane matrix, concomitant with a translation in the headgroup position of the oxidized phospholipid: at zero cholesterol content, its headgroup is shifted to the outside of the DOPC headgroup region, whereas increasing cholesterol concentrations pulls the headgroup into the bilayer plane.

Introduction

Phospholipids containing polyunsaturated fatty acids are highly prone to modification by reactive oxygen species, thereby generating a plethora of biologically active oxidized phospholipids (oxPLs).[1,2] A variety of (patho-) physiological effects ascribed to oxPLs underline their relevance, e.g., in inflammation,[3–5] atherosclerosis,[6] or immune response.[7] The modes of action are diverse. First, different families of receptors were described to become activated due to oxPL binding.[1] Second, oxPLs were shown to interact with drugs, thereby influencing their pharmacokinetics.[8] Finally, one may expect the exceptional structure of an oxPL molecule to affect its biophysical properties in the lipid membrane. In this report, we will focus on the last aspect.

Bioactive oxPLs contain extensively modified or truncated acyl chains in the *sn-2* position, typically terminated by polar carboxylic or aldehydic groups. As was shown by nuclear magnetic resonance, Langmuir balance, and molecular dynamics (MD) simulations, the truncated polar moiety can protrude into the aqueous phase, despite the energy penalty associated with the exposition of the nonpolar chain regions.[9–12] As a consequence, bilayer properties such as permeability, mobility, and headgroup hydration are altered by the addition of oxPLs.[13,14] We have recently studied the diffusional properties of a fluorescent oxPL analogue, 1-palmitoyl-2-glutaroyl-*sn*-glycero-3-phospho-*N*-Alexa647-ethanolamine (PGPE-Alexa647), in the live cell plasma membrane, and found exceptionally high mobility of $\sim 2 \ \mu m^2/s$,[15] in agreement with the expected lysolipid-like behavior. Moreover, we observed transient immobilization at endocytic sites, which we attributed to a preferential partitioning within highly curved membrane regions due to the inverted cone-like shape of the PGPE-Alexa647.[15]

*To whom correspondence should be addressed. Tel.: +43-732-2468-9284. Fax: +43-732-2468-29284. E-mail: gerhard.schuetz@jku.at.

(1) Fu, P.; Birukov, K. G. Oxidized phospholipids in control of inflammation and endothelial barrier. *Transl. Res.* **2009**, *153*(4), 166–76.

(2) Deigner, H. P.; Hermetter, A. Oxidized phospholipids: emerging lipid mediators in pathophysiology. *Curr. Opin. Lipidol.* **2008**, *19*(3), 289–94.

(3) Knapp, S.; Matt, U.; Leitinger, N.; van der Poll, T. Oxidized phospholipids inhibit phagocytosis and impair outcome in gram-negative sepsis in vivo. *J. Immunol.* **2007**, *178*(2), 993–1001.

(4) Bochkov, V. N.; Kadl, A.; Huber, J.; Gruber, F.; Binder, B. R.; Leitinger, N. Protective role of phospholipid oxidation products in endotoxin-induced tissue damage. *Nature* **2002**, *419*(6902), 77–81.

(5) Bochkov, V. N. Inflammatory profile of oxidized phospholipids. *Thromb. Haemost.* **2007**, *97*(3), 348–54.

(6) Mertens, A.; Holvoet, P. Oxidized LDL and HDL: antagonists in athero-thrombosis. *FASEB J.* **2001**, *15*(12), 2073–84.

(7) Seyerl, M.; Bluml, S.; Kirchberger, S.; Bochkov, V. N.; Oskolkova, O.; Majdic, O.; Stockl, J. Oxidized phospholipids induce anergy in human peripheral blood T cells. *Eur. J. Immunol.* **2008**, *38*(3), 778–87.

(8) Mattila, J. P.; Sabatini, K.; Kinnunen, P. K., Oxidized Phospholipids As Potential Novel Drug Targets. *Biophys. J.* **2007**.

(9) Li, X. M.; Salomon, R. G.; Qin, J.; Hazen, S. L. Conformation of an endogenous ligand in a membrane bilayer for the macrophage scavenger receptor CD36. *Biochemistry* **2007**, *46*(17), 5009–17.

(10) Greenberg, M. E.; Li, X. M.; Gugiu, B. G.; Gu, X.; Qin, J.; Salomon, R. G.; Hazen, S. L. The lipid whisker model of the structure of oxidized cell membranes. *J. Biol. Chem.* **2008**, *283*(4), 2385–96.

(11) Khandelia, H.; Mouritsen, O. G. Lipid gymnastics: evidence of complete acyl chain reversal in oxidized phospholipids from molecular simulations. *Biophys. J.* **2009**, *96*(7), 2734–43.

(12) Sabatini, K.; Mattila, J. P.; Megli, F. M.; Kinnunen, P. K. Characterization of Two Oxidatively Modified Phospholipids in Mixed Monolayers with DPPC. *Biophys. J.* **2006**, *90*(12), 4488–4499.

(13) Beranova, L.; Cwiklik, L.; Jurkiewicz, P.; Hof, M.; Jungwirth, P. Oxidation changes physical properties of phospholipid bilayers: fluorescence spectroscopy and molecular simulations. *Langmuir* **2010**, *26*(9), 6140–4.

(14) Wong-Ekkabut, J.; Xu, Z.; Triampo, W.; Tang, I. M.; Tieleman, D. P.; Monticelli, L. Effect of lipid peroxidation on the properties of lipid bilayers: a molecular dynamics study. *Biophys. J.* **2007**, *93*(12), 4225–36.

(15) Rhode, S.; Grurl, R.; Brameshuber, M.; Hermetter, A.; Schutz, G. J. Plasma membrane fluidity affects transient immobilization of oxidized phospholipids in endocytotic sites for subsequent uptake. *J. Biol. Chem.* **2009**, *284*(4), 2258–65.

To better understand the behavior of oxPL-molecules in membranes we decided to further address its properties in well-defined model systems. We used PGPE-Alexa647 as a representative carboxylated oxPL; we have previously shown that this fluorescent analogue mimics closely the behavior of the nonlabeled molecule in living cells.[16] All data were referenced against a conventional headgroup labeled fluorescent phospholipid, dihexadecanoylphosphoethanolamine (DHPE)-Bodipy.

First, we were interested whether the probe displays any preference with respect to the phase state of the membrane. The cellular plasma membrane is believed to be segregated into domains,[17] where a more ordered ("raft-") phase shall coexist with a disordered phase.[18] Generation of phase-separated model membranes has become standard in many laboratories (for reviews see, e.g., refs 19–21) and provided a wealth of insights into the thermodynamics of lipid bilayers.[20,22] Indeed, a few reports confirmed the presence of ordered environments also in the cellular plasma membrane.[23,24] In this study, we found a moderate preference of the PGPE-Alexa647 for the liquid-disordered phase but also significant partitioning into the liquid ordered phase, indicating a rather promiscuous localization.

Second, in order to explain the high mobility of PGPE-Alexa647 observed in the live cell plasma membrane, we further characterized the diffusion constant in various model membranes. Experiments were performed on supported lipid bilayers (SLBs) using line-scan fluorescence correlation spectroscopy (FCS)[25] and single molecule tracking.[26] Substantially higher oxPL mobility was observed consistently; it could be diminished by increasing cholesterol content and intensified by introducing artificial obstacles. We used coarse-grained MD simulations to explain the differential mobilities.

Materials and Methods

Chemicals. 1,2-Dioleoyl-*sn*-glycero-3-phosphocholine (dioleoyl-phosphatidylcholine; DOPC), sphingomyelin from porcine brain (BrSM), *N*-octadecanoyl-D-erythro-sphingosine (C18 ceramide; Cer), and cholesterol were purchased from Avanti Polar Lipids (Alabaster, AL, U.S.A.) and used without further purification. Two different fluorescent lipids were used as probes: *N*-(4,4-difluoro-5, 7-dimethyl-4-bora-3a,4a-diaza-*s*-indacene-3-propionyl)-1,2-dihexadecanoyl-*sn*-glycero-3-phosphoethanolamine and triethylammonium salt (BODIPY FL DHPE, Invitrogen, Carlsbad, CA, U.S.A.); the oxidized phopholipid 1-palmitoyl-2-glutaroyl-sn-glycero-3-phospho-*N*-Alexa647-ethanolamine (PGPE-Alexa647) was synthesized as

described previously.[16] Optical Adhesive 88, used to glue the mica on coverslips, was purchased from Norland Products Inc. (Cranbury, NJ, U.S.A.). Two different buffers were used for sample preparation: buffer A (150 mM NaCl, 10 mM Hepes, and 3 mM NaN3, pH 7.4) and buffer B (PBS-buffer; PAA Pasching, Austria). Buffer A was filtered through a 0.2 μm filter (Nalgene, Rochester, NY, U.S.A.) prior to use. 1,2-Dioleoyl-*sn*-glycero-3-phosphoethanolamine-*N*-(cap biotinyl) (sodium salt) (18:1 Biotinyl Cap PE; DOPE-biotin) was purchased from Avanti Polar Lipids (Alabaster, AL, U.S.A.).

Supported Lipid Bilayers (SLBs). Glass slides (Menzel, #1, Braunschweig, Germany) were incubated in a 3:1 Piranha solution of sulfuric acid (J.T. Baker, 95–97%, New Jersey, U.S.A.) and hydrogen peroxide (Merck, 30%, New Jersey, USA) for 20 min, rinsed with deionized water and ethanol, and dried by nitrogen. Glass slides were then glued on a measurement chamber (Lab-Tek, Nunc, Thermo Fisher Scientific, Rochester) from which the glass support has been removed.

A total of 10 mg of DOPC was dissolved in a mixture of methanol and chloroform (1:3). Then, 10 μL of a 10 mg/mL DOPC solution was evaporated under nitrogen stream and diluted with 100 μL buffer B. Vesicle solutions were prepared by ultrasonicating for 20 min. The accrued vesicle solution was put on a glass slide or avidin-coated surface. After 20 min the bilayer had been formed and was washed with buffer B. Fluorescently labeled lipids were incorporated after bilayer formation by incubation from the aqueous subphase: for this, bilayers were incubated with a 2,5 nM solution of DHPE-Bodipy and with a 5nM solution of PGPE-Alexa647 for another 20 min, followed by thorough washing with buffer B. Avidin-coated glass surfaces were prepared by incubating a Piranha-cleaned glass-coverslip with a 10 mg/mL avidin solution for 20 min, and subsequent washing with buffer B.

Phase Separated Lipid Bilayers (SLBs). DOPC, bSM, and cholesterol were mixed in organic solution (1:3/methanol: chloroform) in a molar ratio of 2:2:1. After solvent evaporation, the lipid film thus obtained was slowly rehydrated using buffer B at 10 mg/mL lipid concentration and resuspended through vigorous vortexing. After sonicating the suspension at 60 °C, a small aliquot was diluted in buffer A and deposited in the presence of 2 mM CaCl$_2$ on a ~10 μm thick, freshly cleaved mica glued onto a glass coverslip. The coverslip was sealed with a home-built polypropylene chamber and incubated at 55 °C for 5 min. After that, the sample was rinsed at the same temperature at least 10 times with buffer A and allowed to cool down to 25 °C. At this stage, fluorescently labeled lipids could be incorporated into the bilayer by addition from the aqueous subphase. The concentration of DHPE-Bodipy was varied between 0.1 to 0.01 mol % and for PGPE-Alexa647 from 0.5 to 0.01 mol %. After 20 min, the sample was rinsed again to remove the fluorescent lipids from the buffer solution.

Single Dye Tracing. Single molecule experiments were performed as described previously.[27] Briefly, a Zeiss Axiovert 200 microscope was equipped with a 100× NA = 1.46 α Plan - APOCHROMAT objective (Zeiss, Oberkochen Germany). Samples were illuminated in objective-type total internal reflection (TIR) configuration via the epiport using 488 nm light from an Ar+ laser (model 2017-05AR, Spectra Physics, Mountain View, CA, U.S. A.) with an intensity of typically 9–11 kW/cm^2 and 647 nm light from a Kr+ laser (Stabilite 2017-KR, Spectra Physics) with intensities of typically 5–10 kW/cm^2. A slit aperture (Zeiss) with a width of ~7 μm in the object plane was used as field stop to confine the illumination area. After appropriate filtering (Z488 647MV2, Z488 647RPC, Chroma, VT, U.S.A.), emitted signals were split into two color channels using a custom-made dichroic wedge (Chroma) and imaged on the same back-illuminated, liquid-nitrogen-cooled CCD camera (Micro Max 1300-PB,

(16) Moumtzi, A.; Trenker, M.; Flicker, K.; Zenzmaier, E.; Saf, R.; Hermetter, A. Import and fate of fluorescent analogs of oxidized phospholipids in vascular smooth muscle cells. *J. Lipid Res.* **2007**, *48*(3), 565–82.

(17) Pike, L. J. Rafts Defined. *J. Lipid Res.* **2006**, *47*(7), 1597–1598.

(18) Brown, D. A.; London, E. Structure and origin of ordered lipid domains in biological membranes. *J. Membr. Biol.* **1998**, *164*(2), 103–14.

(19) de Almeida, R. F. M.; Loura, L. M. S.; Prieto, M. Membrane lipid domains and rafts: current applications of fluorescence lifetime spectroscopy and imaging. *Chem. Phys. Lipids* **2009**, *157*(2), 61–77.

(20) Veatch, S. L.; Keller, S. L. Seeing spots: complex phase behavior in simple membranes. *Biochim. Biophys. Acta* **2005**, *1746*(3), 172–85.

(21) Simons, K.; Vaz, W. L. Model systems, lipid rafts, and cell membranes. *Annu. Rev. Biophys. Biomol. Struct.* **2004**, *33*, 269–95.

(22) Feigenson, G. W. Phase boundaries and biological membranes. *Annu. Rev. Biophys. Biomol. Struct.* **2007**, *36*, 63–77.

(23) Swamy, M. J.; Ciani, L.; Ge, M.; Smith, A. K.; Holowka, D.; Baird, B.; Freed, J. H. Coexisting Domains in the Plasma Membranes of Live Cells Characterized by Spin-Label ESR Spectroscopy. *Biophys. J.* **2006**, *90*(12), 4452–65.

(24) Gaus, K.; Gratton, E.; Kable, E. P.; Jones, A. S.; Gelissen, I.; Kritharides, L.; Jessup, W. Visualizing lipid structure and raft domains in living cells with two-photon microscopy. *Proc. Natl. Acad. Sci. U.S.A.* **2003**, *100*(26), 15554–9.

(25) Ries, J.; Chiantia, S.; Schwille, P. Accurate determination of membrane dynamics with line-scan FCS. *Biophys. J.* **2009**, *96*(5), 1999–2008.

(26) Schmidt, T.; Schütz, G. J.; Baumgartner, W.; Gruber, H. J.; Schindler, H. Imaging of single molecule diffusion. *Proc. Natl. Acad. Sci. U.S.A.* **1996**, *93*(7), 2926–9.

(27) Wieser, S.; Schütz, G. J. Tracking single molecules in the live cell plasma membrane-Do's and Don'ts. *Methods* **2008**, *46*(2), 131–40.

Roper Scientific, Trenton, NJ, U.S.A.). For the precise control of all laser pulse trains, an acoustic-optical modulator (1205C, Isomet, Springfield, VA, U.S.A.) was used. Timing protocols were generated and controlled by an in-house program package implemented in LABVIEW (National Instruments, Austin, TX, U.S.A.). Illumination times were adjusted to values between 1 and 3 ms. Movies were recorded with a delay of 2 ms between two consecutive images. Experiments were performed in a home-built incubator box equipped with a heating unit, a temperature-adjustable stage insert and an objective heater (Pecon, Erbach, Germany). Signals were analyzed by fitting a two-dimensional Gaussian profile, yielding the position with an accuracy of ∼50 nm. The sample was mounted on a high-precision XY-stage (Scan IM 120 × 100, Märzhäuser, Germany).

Data Analysis. For single molecule analysis, images were analyzed using in-house algorithms implemented in MATLAB (MathWorks, Natick, MA, U.S.A.).[27] Individual diffraction limited signals were selected and fitted with a Gaussian profile, yielding the single molecule position, the brightness B and the full width at half-maximum (fwhm) of the Gaussian function.

Single molecule mobility was analyzed as described previously.[27] In brief, trajectories are specified by a sequence of positions $\vec{x}(t)$, with i ranging from 1 to the number of observations of this trajectory. The mean square displacements $\langle r^2 \rangle$ were calculated as a function of the time-lag $t_{lag} = n(t_{ill} + t_{delay})$ according to $\langle r^2 \rangle = \langle \vec{x}(t + t_{lag}) - \vec{x}(t) \rangle^2$, with n denoting the difference in frame index. Estimated data were analyzed by fitting with the function

$$\langle r^2 \rangle = 4Dt_{lag} + 4\sigma^2 \qquad (1)$$

yielding the lateral diffusion constant D and the single molecule localization precision σ. Only the first two data-points were used for the linear fit.[27]

Line-Scan Fluorescence Correlation Spectroscopy. Line-scan fluorescence correlation spectroscopy (LSFCS) was performed at room temperature (25 °C) on a LSM 510 Meta (Zeiss, Jena, Germany) as described in ref 25. The fiber output was coupled to a home-built FCS detection unit, consisting of an emission filter and an achromatic doublet (Linos Photonics, Goettingen, Germany), to image the internal pinhole onto the optical fiber connected to an avalanche photodiode (APD) (Perkin-Elmer, Boston, MA, U.S.A.). Correlation curves were obtained with a hardware correlator (Correlator.com, Bridgewater, NJ, U.S.A.). For confocal fluorescence microscopy, the excitation light of an argon laser at 488 nm (or a He−Ne laser at 543 nm) was reflected by a dichroic mirror (HFT 488/543/633) and focused onto the sample by a Zeiss C-Apochromat 40×, NA) 1.2, UV−vis−IR water immersion objective. The fluorescence signal was then recollected by the same objective and, after passing through a 525/50 bandpass filter (or a 580/60 bandpass filter), measured by a photomultiplier (PMT). The confocal geometry was ensured by a 70 μm (80 μm) pinhole in front of the PMT. FCS measurements were performed using the same optical path described for the fluorescence imaging, the signal from the sample being collected in this case by the avalanche photodiodes in the FCS unit.

Molecular Dynamics Simulations. The membranes simulated in this work consisted of 2500 lipids per leaflet and contained 50 water molecules per lipid (corresponding to 12.5 water beads in the coarse grained representation). The main lipid in the bilayer is DOPC. The content of cholesterol was increased from 0% to 50% by substituting DOPC with cholesterol. Additionally, 1% of the lipid molecules was the oxidized lipid 1-palmitoyl-2-glutaroyl-*sn*-glycero-3-phosphocholine (PGPC) introduced by substituting DOPC with PGPC (Figure 4A). Counterions were added randomly to electroneutralize the system.

During bilayer construction the lipids were randomly placed in the plain of the bilayer and rotated using an axis normal to the membrane. Atom overlaps were resolved by first expanding the

bilayer in the membrane plane, followed by a size reduction in small steps to the typical area per lipid of a DOPC-cholesterol mixture, involving energy minimization and geometry optimization for each deflation step.[28] The systems was further equilibrated by first carrying out 10 and 50 ns equilibration runs with first restraining in Z the phosphate of the phospholipids and the polar oxygen of the cholesterol and then only restraining the phospholipids. After 100 ns of unconstrained equilibration we carried out a production run of 200 ns. We used the coarse grained Martini force field.[29,30] The parameters of the oxidized tail of the PGPC lipid were extracted from all atom simulations of PGPC in 1-palmitoyl-2-oleoyl-sn-glycero-3-phosphocholine (POPC) using Berger lipids,[31] missing parameters were taken from the force field and from Wong-Ekkabut et al.[14] and using the SPC water model.[32] The truncated oxidized glycero-lipid tail was coarse grained into two beads, one containing the charged carboxy terminus, one consisting of the aliphatic carbons of the chain. The 50 ns all atom trajectory was converted into coarse grained representation. Bead distances and bond and dihedral angles were measured and added to the coarse grained description of PGPC. All simulations were performed using the Gromacs 4.0.5 MD package.[33,34] The integration time step was set to 20 fs. Periodic boundary conditions were applied in all dimensions. A constant temperature of 310 K was maintained using the velocity rescale (v-rescale) algorithm[35] with a coupling time of 0.3 ps, coupling independently the water and the lipids plus ions to an external bath. A pressure of 1 bar was maintained in both the membrane plane and the membrane normal, using semi-isotropic Berendsen pressure coupling scheme[36] with a time constant of 3 ps. A shift function was applied to the van der Waals interactions between 0.9 and 1.2 nm, and the electrostatic interactions were shifted over the entire range from 0 to 1.2 nm. Diffusion constants were calculated by fitting the linear part of the mean square displacment curves with $\langle r^2 \rangle = 4Dt_{lag}$, after removing overall translation by fitting of the DOPC molecules. It is a known limitation of the coarse grained Martini force field that on an absolute scale the velocity of molecules are overestimated and scaling up an order of magnitude has been suggested.[29] We applied a scaling factor of 15 to obtain accordance on the absolute scale of the experimentally observed diffusion rates. The density profiles were calculated using standard procedures[37,38] after removing translational shifts of the membranes, which were determined from the mean position of all DOPC headgroups. The positions of the PGPC and DOPC phosphate groups along the membrane normal were extracted

(28) Kandt, C.; Ash, W. L.; Tieleman, D. P. Setting up and running molecular dynamics simulations of membrane proteins. *Methods* 2007, *41*(4), 475–88.
(29) Marrink, S. J.; Risselada, H. J.; Yefimov, S.; Tieleman, D. P.; de Vries, A. H. The MARTINI force field: coarse grained model for biomolecular simulations. *J. Phys. Chem. B* 2007, *111*(27), 7812–24.
(30) Marrink, S. J.; de Vries, A. H.; Mark, A. E. Coarse grained model for semiquantitative lipid simulations. *J. Phys. Chem. B* 2004, *108*(2), 750–760.
(31) Berger, O.; Edholm, O.; Jahnig, F. Molecular dynamics simulations of a fluid bilayer of dipalmitoylphosphatidylcholine at full hydration, constant pressure, and constant temperature. *Biophys. J.* 1997, *72*(5), 2002–13.
(32) Berendsen, H. J. C.; Postma, J. P. M.; Van Gunsteren, W. F.; Hermans, J. Interaction models for water in relation to protein hydration. In *Intermolecular Forces*, Pullman, B., Ed.; D Reidel Publishing Company: Dordrecht, The Netherlands, 1981; pp 331−342.
(33) Hess, B.; Kutzner, C.; van der Spoel, D.; Lindahl, E. GROMACS 4: Algorithms for highly efficient, load-balanced, and scalable molecular simulation. *J. Chem. Theory Comput.* 2008, *4*(3), 435–447.
(34) Van der Spoel, D.; Lindahl, E.; Hess, B.; Groenhof, G.; Mark, A. E.; Berendsen, H. J. C. GROMACS: Fast, flexible, and free. *J. Comput. Chem.* 2005, *26*(16), 1701–1718.
(35) Bussi, G.; Donadio, D.; Parrinello, M. Canonical sampling through velocity rescaling. *J. Chem. Phys.* 2007, *126*(1), 014101.
(36) Berendsen, H. J. C.; Postma, J. P. M.; Vangunsteren, W. F.; Dinola, A.; Haak, J. R. Molecular-Dynamics with Coupling to an External Bath. *J. Chem. Phys.* 1984, *81*(8), 3684–3690.
(37) Tieleman, D. P.; Marrink, S. J.; Berendsen, H. J. A computer perspective of membranes: molecular dynamics studies of lipid bilayer systems. *Biochim. Biophys. Acta* 1997, *1331*(3), 235–70.
(38) Marrink, S. J.; Sok, R. M.; Berendsen, H. J. C. Free volume properties of a simulated lipid membrane. *J. Chem. Phys.* 1996, *104*(22), 9090–9099.
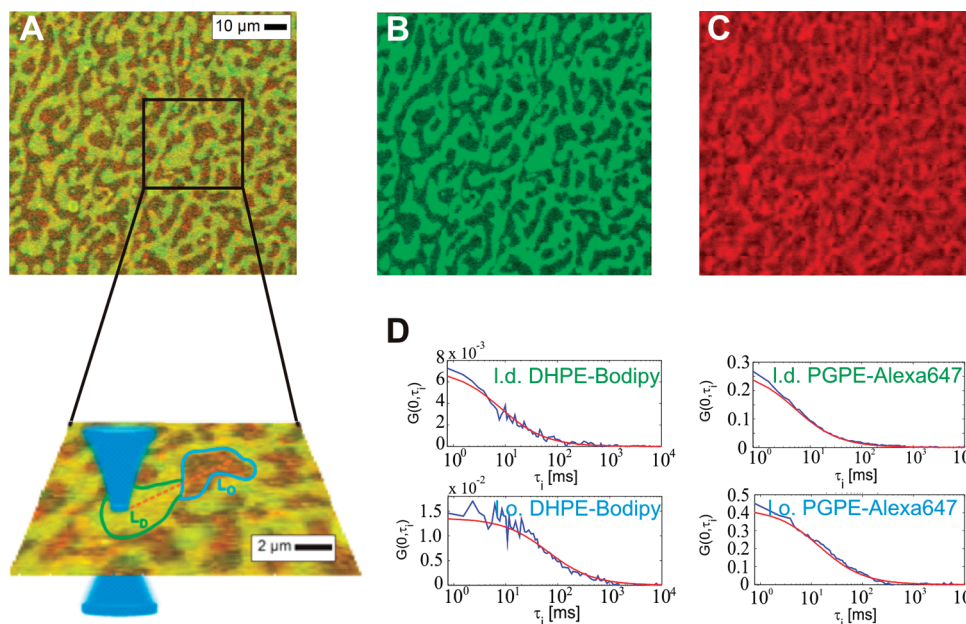
Figure 1. Partitioning and mobility of PGPE-Alexa647 and DHPE-Bodipy in phase-separated supported lipid bilayers. Panels A−C show confocal fluorescence images of a DOPC/bSM/Chol 2:2:1 supported bilayer doped with trace amounts DHPE-Bodipy and PGPE-Alexa647: an overlay, the Bodipy-channel and the Alexa647-channel are shown in panels A−C, respectively. Phase separation into l.o. and l.d. domains is clearly visible due to the exclusion of DHPE-Bodipy. We performed line-scan FCS to quantify partition coefficients and mobilities (sketch in the inset to A: the blue cone shows the detection volume, the blue and green encircled areas correspond to the l.o. and l.d. phases; the orange dotted line represents the FCS line scan). (D) Representative averaged autocorrelation curves measured in different lipid phases of the bilayer at room temperature. Shown are autocorrelation curves for the l.d. phase (upper figures) and the l.o. phase (bottom figures) for the two different probes DHPE-Bodipy (left) and PGPE-Alexa647 (right). Data were fitted for two-dimensional diffusion, yielding the diffusion constants D and the surface densities σ. The obtained fit values are listed in Table1.

Table 1. Partition Coefficients and Diffusion Constants on Phase Separated Bilayers[a]

lipid composition	phase	$D_{\text{DHPE-Bodipy}}$ [μm^2/s]	$D_{\text{PGPE-Alexa647}}$ [μm^2/s]	$K_{\text{DHPE-Bodipy}}$	$K_{\text{PGPE-Alexa647}}$
bSM:DOPC:cholesterol 2:2:1	l.d.	2.86 (0.13)	3.73 (0.094)	0.319	0.749
	l.o.	0.34 (0.022)	0.78 (0.050)		
bSM:DOPC:cholesterol:ceramide 0.7:1:0.67:0.3	l.d.	2.17 (0.058)	2.21 (0.037)	$\sigma_{\text{cer}}/\sigma_{\text{ld}} = 0.004$	$\sigma_{\text{cer}}/\sigma_{\text{ld}} = 0.01$
	cer				

[a] Standard errors of the mean are given in parentheses.

from the density plots by fitting the phosphate group density peak with a Gaussian function (Figure 5).

Distances between each phospholipid molecule (represented by its phosphate group) and the nearest cholesterol molecule (represented by its hydroxyl group) were calculated for each time point within a trajectory (Figure 6). The resulting histograms (bin-width 0.02 nm) were averaged for all phospholipids in the simulation.

Results

To address the phase preference of PGPE-Alexa647, we studied its partitioning in supported lipid bilayers containing bSM:DOPC:Chol in a molar ratio of 2:2:1 (Figure 1), which shows separation in liquid ordered (l.o.) and disordered (l.d.) phase.[39] PGPE-Alexa647 and DHPE-Bodipy were added from the aqueous phase to ensure that the probes inserted only in the upper leaflet; flip-flop is too slow to yield probe redistribution between leaflets during the experimental time frame of less than 1 h.[40] While the DHPE-Bodipy was largely excluded from the

ordered phase (green color channel), we observed only weak contrast for PGPE-Alexa647. We performed line-scan FCS to determine accurate values of the surface densities in the ordered (σ_{lo}) versus the disordered phase (σ_{ld}), yielding the partition coefficients $K = \sigma_{\text{lo}}/\sigma_{\text{ld}}$ for PGPE-Alexa647 ($K = 0.75$) and for DHPE-Bodipy ($K = 0.32$) (see Table 1). We also calculated the diffusion constants of the probe molecules, yielding higher mobility of the oxidized phospholipid analogue versus DHPE-Bodipy in both phases (Table 1).

The rather high l.o.-phase partitioning of PGPE-Alexa647 lead us to the hypothesis that ordered phases in general may be well accessible by the oxPL. We thus investigated a bilayer composed of bSM:DOPC:Chol:Cer in a molar ratio of 0.64:1:1:0.36, which yields a two phase equilibrium between a ceramide-enriched gel-like phase and a liquid disordered phase.[41] Previous data revealed efficient exclusion of all investigated fluorescent analogues.[42] We indeed confirmed reduced partitioning into the ceramide-enriched phase for both probes. Due the low partitioning, we estimated the surface densities directly from the confocal images: a partition

(39) Kahya, N.; Scherfeld, D.; Bacia, K.; Poolman, B.; Schwille, P. Probing lipid mobility of raft-exhibiting model membranes by fluorescence correlation spectroscopy. *J. Biol. Chem.* **2003**, *278*(30), 28109–15.

(40) Kiessling, V.; Crane, J. M.; Tamm, L. K. Transbilayer effects of raft-like lipid domains in asymmetric planar bilayers measured by single molecule tracking. *Biophys. J.* **2006**, *91*(9), 3313–26.

(41) Chiantia, S.; Kahya, N.; Ries, J.; Schwille, P. Effects of ceramide on liquid-ordered domains investigated by simultaneous AFM and FCS. *Biophys. J.* **2006**, *90*(12), 4500–8.

(42) Chiantia, S.; Ries, J.; Chwastek, G.; Carrer, D.; Li, Z.; Bittman, R.; Schwille, P. Role of ceramide in membrane protein organization investigated by combined AFM and FCS. *Biochim. Biophys. Acta* **2008**, *1778*(5), 1356–64.
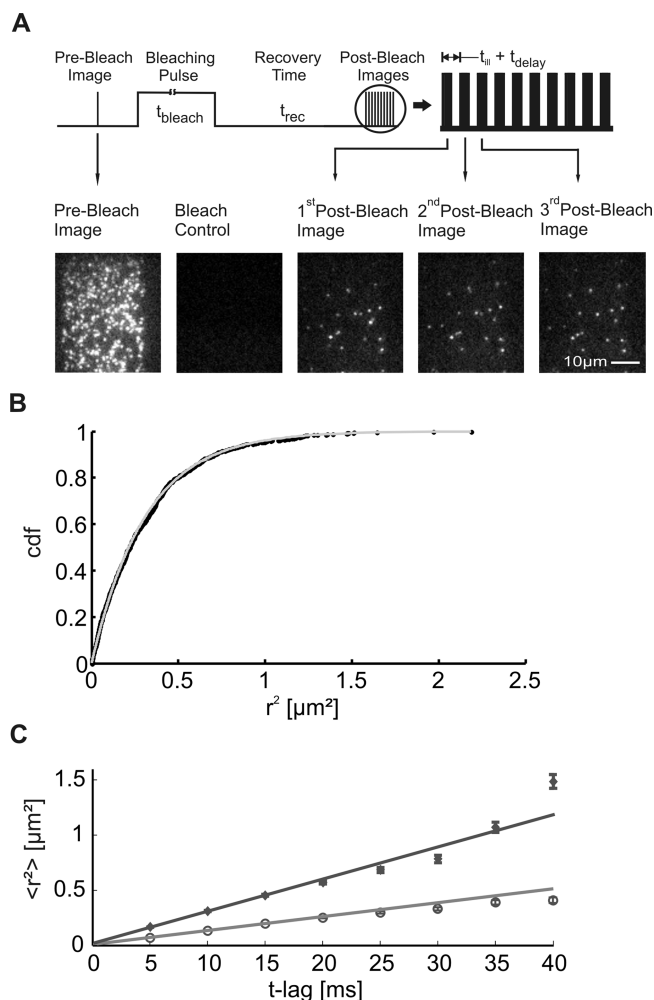
Figure 2. Single molecule tracking in supported DOPC bilayers. (A) The upper row sketches the applied laser timing protocol, the lower row an example of an image sequence. After recording a prebleach image the according area was totally photobleached by applying a laser pulse for $t_{bleach} \sim 250$ ms. The photobleaching efficiency was controlled by recording an image immediately after the bleach pulse. After a recovery time of $t_{rec} \sim 2000$ ms, single fluorescently labeled lipids entering the field of view can be resolved as diffraction limited signals. By recording an image sequence with high time resolution ($t_{ill} = 3$ ms, $t_{delay} = 2$ ms) individual lipids can be tracked over multiple images for determination of their diffusion constant. Panel B shows the cumulative density function *cdf* of square displacements between consecutive images at $t_{lag} = 10$ ms for PGPE-Alexa647. The monoexponential behavior confirms the presence of just a single mobile fraction. (C) Exact values for diffusion constants *D* were calculated by plotting $\langle r^2 \rangle$ versus t_{lag}, and fitting with eq 1. A clear difference for *D* is observed by comparing PGPE-Alexa647 (dark gray line, $D = 7.2 \pm 0.22$ $\mu m^2/s$) and DHPE-Bodipy (gray line, $D = 3.1 \pm 0.09$ $\mu m^2/s$). Experiments were performed at 37 °C.

coefficient of $\sigma_{cer}/\sigma_{ld} = 0.004$ was calculated for DHPE-Bodipy; yet, also in this case ceramide-phase partitioning of PGPE-Alexa647 was significantly higher ($\sigma_{cer}/\sigma_{ld} = 0.01$). Mobility in the l.d. phase was reduced compared to the ternary system for both probes, and the mobility difference basically vanished (Table 1). Probe mobility in the ceramide-enriched gel-like phase was too low to be measurable. In summary, the oxidized lipid analogue shows rather weak phase preference; in general, its mobility is higher than the mobility of a conventional phospholipid.

We continued by putting our focus on the mobility difference between PGPE-Alexa647 and DHPE-Bodipy. Glass-supported
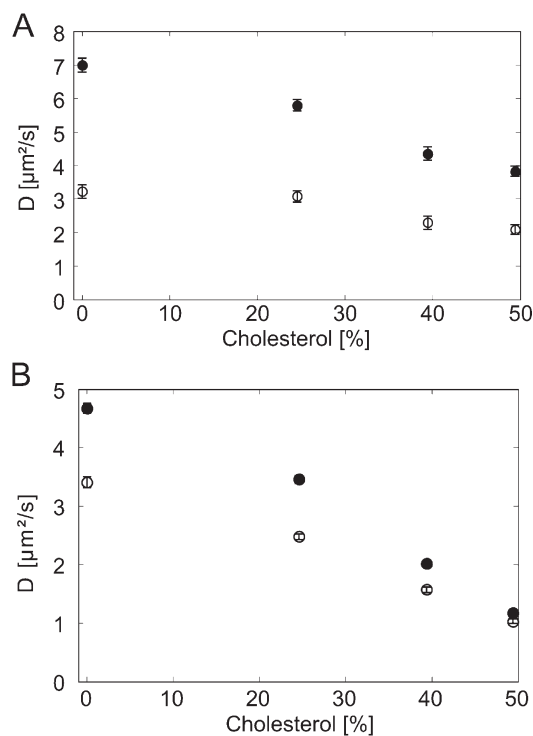

Figure 3. Diffusion constant of DHPE and PGPE in a DOPC/cholesterol bilayer as a function of cholesterol content, determined by single molecule tracking. DOPC bilayers containing up to 50% cholesterol were labeled with PGPE-Alexa647 (full circles) and DHPE-Bodipy (open circles). Experiments were performed at 37 °C (A) or 25 °C (B).

lipid bilayers of DOPC were prepared and studied at 25 or 37 °C. After bilayer formation, PGPE-Alexa647 and DHPE-Bodipy were added from the aqueous phase. We used single molecule tracking to determine the diffusion constant of both lipid analogues in the same bilayer regions. To eliminate potential influences due to the immobilization of molecules at surface defects we started each recording sequence by a photobleaching pulse, which irreversibly destroyed all fluorophores in the field of view (Figure 2A). After a recovery time of 0.5−2 s, unbleached fluorescent lipid molecules have entered the field of view and could be tracked. By this measurement mode, we could restrict the analysis to a clean fraction of freely diffusing probe molecules. For our experiments, we used stroboscopic illumination with a time delay of $t_{del} = 2$ ms between two consecutive illumination pulses and an illumination time $t_{ill} = 1$ or 3 ms. From the single molecule trajectories, the distribution of step sizes was determined and further analyzed to assess potential heterogeneity in the sample mobility, which would yield deviations from a monoexponential behavior.[43−45] However, we found here for all bilayers and probe molecules purely monoexponential functions (exemplified in Figure 2B). We also tested for anomalous subdiffusion behavior, being indicative for confinements of the tracer or nonequilibrated systems:[27] when plotting the mean square displacement ($\langle r^2 \rangle$) as function of the time-lag (t_{lag}), anomalous subdiffusion would yield a sublinear increase. However, for all data sets we found perfectly linear

(43) Schütz, G. J.; Schindler, H.; Schmidt, T. Single-molecule microscopy on model membranes reveals anomalous diffusion. *Biophys. J.* **1997**, *73*(2), 1073–80.
(44) Sonnleitner, A.; Schutz, G. J.; Schmidt, T. Free brownian motion of individual lipid molecules in biomembranes. *Biophys. J.* **1999**, *77*(5), 2638–42.
(45) Wieser, S.; Axmann, M.; Schütz, G. J. Versatile analysis of single-molecule tracking data by comprehensive testing against Monte Carlo simulations. *Biophys. J.* **2008**, *95*(12), 5988–6001.
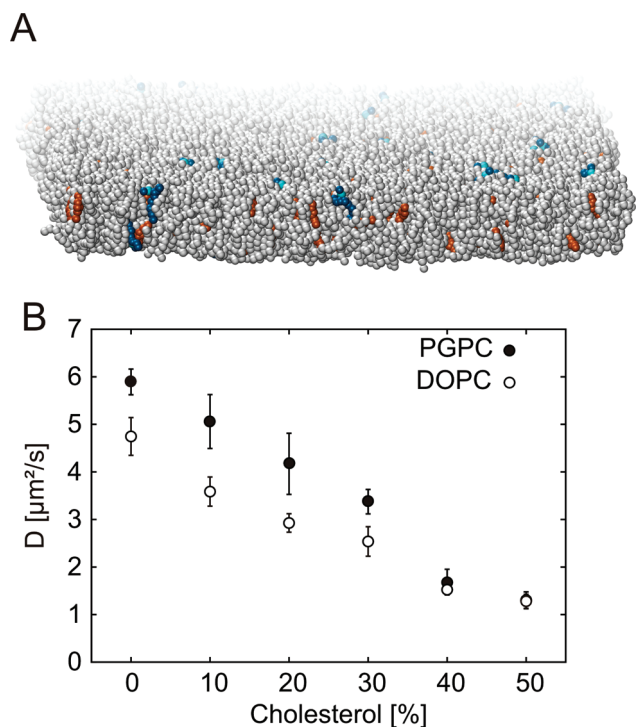
Figure 4. Molecular dynamics simulations of DOPC bilayers containing 1% PGPC and varying concentrations of cholesterol. (A) Snapshot of the system at 20% cholesterol. DOPC is show in gray, PGPC is show in blue (phosphate group in light blue), and cholesterol is show in orange. (B) Effects of increasing cholesterol on the lateral diffusion of PGPC (full circles) and DOPC (open circles). The diffusion was scaled to the experimentally determined range.

relationships (exemplified in Figure 2C). From the slopes, the diffusion constants were calculated according to eq 1. We found substantially higher mobility for PGPE-Alexa647 compared to DHPE-Bodipy (Figure 3): at 25 °C the oxPL showed a ~1.3-fold higher diffusion constant than the conventional phospholipid, at 37 °C we found even a ratio of ~2.2. Interestingly, this difference was reduced and finally disappeared for DOPC bilayers containing increasing amounts of cholesterol (Figure 3).

To understand this behavior, we performed coarse-grained MD simulations of a DOPC matrix containing low concentrations of PGPC and varying concentrations of cholesterol. Figure 4A shows a snapshot of the membrane: consistent with previous all-atom simulations on similar compounds,[11,13,14] we observed the reversal of the truncated acyl-chain in the sn-2 position of PGPC, which frequently protruded out of the membrane into the aqueous subphase. This phenomenon was present for all cholesterol concentrations. No aggregation or alignments of the analyzed lipids was observable on length scales > 5 nm, indicating that influences of potential membrane undulations can be neglected.[46] We determined the diffusion coefficient for both DOPC and PGPC by calculating $\langle r^2 \rangle$ and fitting to the linear region according to $\langle r^2 \rangle = 4Dt_{\mathrm{lag}}$. At zero cholesterol we observed a 1.4-fold higher mobility of the oxPL PGPC compared to the matrix lipid DOPC, similar to our experimental data recorded at 25 °C. Since PGPC carries essentially only one chain that is inserted into the hydrophobic core of the membrane, the consequentially small area of the lipid appears to be responsible for its high mobility.

(46) Goetz, R.; Gompper, G.; Lipowsky, R. Mobility and elasticity of self-assembled membranes. *Phys. Rev. Lett.* **1999**, *82*(1), 221–224.
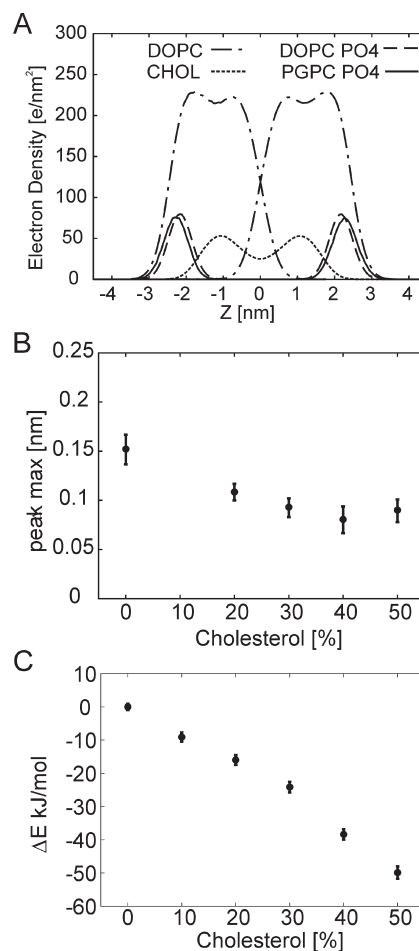
Figure 5. Electron density profiles extracted from the MD trajectories. (A) Total electron density profiles of DOPC and cholesterol are shown along with the electron density of the phosphate groups of PGPC and DOPC, which are scaled for better visualization. Data are shown for 20% cholesterol. (B) We calculated the peak-shift in the maxima of the phosphate groups for DOPC versus PGPC, which is shown as function of cholesterol concentration. Error bars were determined by comparing peak position of the first half of the trajectory with the second half and by differences in peak to peak distances between upper and lower leaflets. (C) The cumulative potential energy of interaction with all membrane components per PGPC molecule is shown relative to the value obtained at 0% cholesterol content. Addition of cholesterol to the membrane increases the interaction strength while no changes where observed for interaction with the aqueous phase (not shown).

Strikingly, the simulations also revealed a convergence of the mobility ratio to 1 with increasing cholesterol concentrations (Figure 4B), in perfect agreement to our experimental data. Electron density profiles gave a first hint on the origin of the effect (Figure 5). At zero cholesterol content, the PGPC head-group region (indicated by the phosphate group) is shifted away from the bilayer center by ~1.5 Å compared to the DOPC headgroup region. This effect diminished with increasing cholesterol concentration down to a shift of ~0.8 Å at 40% cholesterol. Apparently, cholesterol facilitates the incorporation of the oxPL within the lipid bilayer. The mean interaction energy between PGPC and the host matrix increased linearly with increasing cholesterol concentration (Figure 5C), indicating an improved accommodation of the oxPL in the membrane. Taken together, the simulations indicate that increasing cholesterol content leads to a shift of PGPC toward the bilayer center, which is accompanied by facilitated contacts and stronger interactions with the
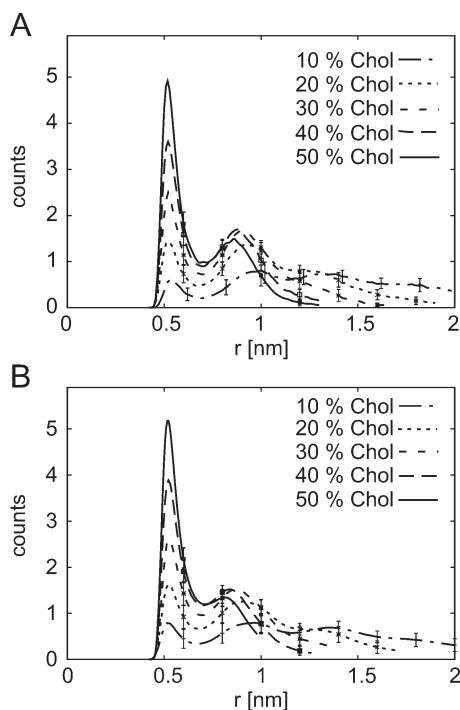
Figure 6. Distribution of distances r between each phospholipid molecule (represented by its phosphate group) and the nearest cholesterol molecule (represented by its hydroxyl group). Plots represent averages over the entire trajectory and over all phospholipids of (A) PGPC and (B) DOPC. Bin-width is 0.02 nm. Standard deviation is shown for every 10th data point.

host lipids and consequentially an adaption of the mobility values between probe and matrix molecules.

We also analyzed the average distance of DOPC or PGPC to their nearest cholesterol molecule (Figure 6). Two peaks are clearly visible: the first one representing probe molecules with directly bound cholesterol and the second one representing probe molecules that are shielded by DOPC from the nearest cholesterol. For DOPC, two effects can be observed when increasing the cholesterol concentration: the first peak gets more pronounced, as the likelihood for direct contact with cholesterol increases, and the distance to the second peaks gets smaller, reflecting the condensing effect of cholesterol.[47,48] The plots for PGPC look qualitatively similar but reveal distinct features. First, in contrast to DOPC, the first peak is substantially lower than the second peak at low cholesterol concentrations; the ratios approach the DOPC-case at high cholesterol content. This means that PGPC has a smaller preference for being associated with cholesterol than with DOPC, most visible at low cholesterol content. Second, the location of the second peak does not shift as strongly as for DOPC, indicating that the condensing effect in the immediate proximity of PGPC is less pronounced.

In summary, high cholesterol concentrations level out the differences in the mobility of oxPL and conventional lipids. It is thus difficult to reconcile the exceptionally high mobility of PGPE-Alexa647 in the plasma membrane ($D = 1.3-2.4\ \mu m^2/s$[15]) with the high native cholesterol concentrations of 30–40%. In comparison, standard lipids or lipid-anchored proteins show a

mobility which is 5- to 10-fold lower.[49–52] We suspected that the diffusion matrix in the plasma membrane may be highly structured, providing essentially a percolation matrix. To enforce this effect in our model system, we artificially introduced obstacles in the proximal leaflet by immobilizing a substantial fraction of lipids. Interleaflet coupling should transmit the effect to the distal leaflet.[53] For this, a DOPC bilayer containing 4.2 mol % Biotin-DOPE was prepared on a glass surface coated with avidin. While PGPE-Alexa647 mobility was reduced only approximately 2-fold, DHPE-Bodipy became basically immobile (Figure 7A,C). Consistently, addition of 40 mol % cholesterol substantially decreased the mobility of PGPE-Alexa647 (Figure 7D). The presence of DOPE-Biotin did not influence the mobility of PGPE-Alexa647 or DHPE-Bodipy in a DOPC bilayer on pure glass (Figure 7B).

Discussion

We studied partitioning and mobility of the oxidized phospholipid PGPE-Alexa647 with reference to the conventional phospholipid DHPE-Bodipy in different lipid membranes. In summary, we made the following observations:

(i) PGPE-Alexa647 shows only marginal preference for fluid versus ordered phases. In general, conventional phospholipids show altered phase partitioning compared to one chain lipids (compare refs 54 and 55). It is tempting to follow an argument of the Vaz group, who ascribed the rate-limiting step for association of a lyso-lipid with a bilayer to the formation of free area with appropriate size in the membrane surface.[55] For the oxPL, single chain insertion is sufficient for thermodynamic equilibrium,[11] therefore the formation of a marginal free area will be sufficient for insertion of PGPE-Alexa647. The data thus indicate that both l.o. and l.d. phase show similar susceptibility for the formation of free area on the length scale of a single acyl chain cross sectional area.

(ii) PGPE-Alexa647 moves faster than DHPE-Bodipy in a supported DOPC bilayer. Substantial mobility differences were observed both experimentally and theoretically. MD simulations revealed that PGPC slightly sticks out of the headgroup region, thereby essentially reducing its effective area, which most likely causes the enhanced mobility.[56] The experimental data show that the effect was more pronounced at elevated temperature, indicating that the shift of PGPC out of the bilayer plane is entropically favored.

(47) Alwarawrah, M.; Dai, J.; Huang, J. A Molecular View of the Cholesterol Condensing Effect in DOPC Lipid Bilayers. *J Phys Chem B* **2010**, *114*, 7516–7523.

(48) Edholm, O.; Nagle, J. F. Areas of molecules in membranes consisting of mixtures. *Biophys. J.* **2005**, *89*(3), 1827–32.

(49) Tank, D. W.; Wu, E. S.; Webb, W. W. Enhanced molecular diffusibility in muscle membrane blebs: release of lateral constraints. *J. Cell Biol.* **1982**, *92*(1), 207–12.
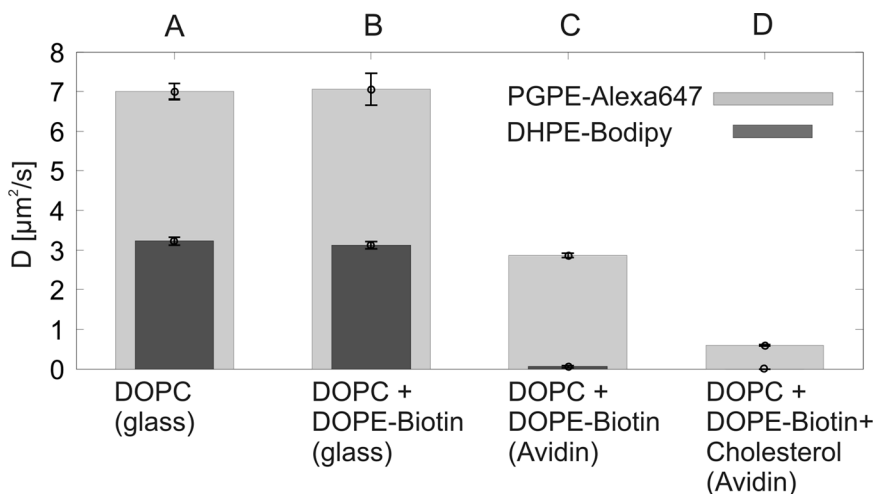
(50) Umemura, Y. M.; Vrljic, M.; Nishimura, S. Y.; Fujiwara, T. K.; Suzuki, K. G.; Kusumi, A. Both MHC class II and its GPI-anchored form undergo hop diffusion as observed by single-molecule tracking. *Biophys. J.* **2008**, *95*, 435–450.

(51) Wieser, S.; Moertelmaier, M.; Fuertbauer, E.; Stockinger, H.; Schütz, G. J. (Un)Confined Diffusion of CD59 in the Plasma Membrane Determined by High-Resolution Single Molecule Microscopy. *Biophys. J.* **2007**, *92*(10), 3719–28.

(52) Kenworthy, A. K.; Nichols, B. J.; Remmert, C. L.; Hendrix, G. M.; Kumar, M.; Zimmerberg, J.; Lippincott-Schwartz, J. Dynamics of putative raft-associated proteins at the cell surface. *J. Cell Biol.* **2004**, *165*(5), 735–46.

(53) Deverall, M. A.; Garg, S.; Ludtke, K.; Jordan, R.; Ruhe, J.; Naumann, C. A. Transbilayer coupling of obstructed lipid diffusion in polymer-tethered phospholipid bilayers. *Soft Matter* **2008**, *4*(9), 1899–1908.

(54) Abreu, M. S.; Moreno, M. J.; Vaz, W. L. Kinetics and thermodynamics of association of a phospholipid derivative with lipid bilayers in liquid-disordered and liquid-ordered phases. *Biophys. J.* **2004**, *87*(1), 353–65.

(55) Sampaio, J. L.; Moreno, M. J.; Vaz, W. L. C. Kinetics and Thermodynamics of Association of a Fluorescent Lysophospholipid Derivative with Lipid Bilayers in Liquid-Ordered and Liquid-Disordered Phases. *Biophys. J.* **2005**, *88*(6), 4064–4071.

(56) Almeida, P. F.; Vaz, W. L.; Thompson, T. E. Lateral diffusion in the liquid phases of dimyristoylphosphatidylcholine/cholesterol lipid bilayers: a free volume analysis. *Biochemistry* **1992**, *31*(29), 6739–47.

Figure 7. Lipid diffusion in obstructed environments. Bilayers were prepared on glass supports (A and B) or glass supports coated with avidin (C and D). Diffusion constants were determined for PGPE-Alexa647 (light gray bars) and DHPE-Bodipy (dark gray bars). Experiments were performed on bilayers of DOPC (A), DOPC containing 4.2 mol % Biotin-DOPE (B and C), or bilayers containing 4.2% Biotin-DOPE and 40% cholesterol (D). Experiments were performed at 37 °C.

(iii) Increased cholesterol concentration reduces the observed mobility differences. In supported DOPC bilayers, increased cholesterol concentration reduced the ratio of diffusion constants (Figure 3). MD simulations of a DOPC matrix containing varying cholesterol content and low amounts of PGPC allowed us to further elucidate the effect of cholesterol on PGPC mobility. At low cholesterol concentrations, PGPC is preferentially surrounded by DOPC, and its headgroup protrudes out of the headgroup region of the DOPC matrix. With increasing cholesterol content, a higher rate of association of PGPC with cholesterol could be observed. Thereby the PGPC headgroup is pulled into the bilayer, with the effect of increasing its interactions with the host lipids and decreasing its mobility.

Moreover, in a four component mixture of bSM: DOPC:Chol:Cer (0.64:1:1:0.36), we found hardly any difference in the l.d. phase mobility of the two probe molecules. We attribute the disappearance of mobility differences to a higher cholesterol concentration in the l.d. phase; indeed, ceramide is known to displace cholesterol from the l.gel phase,[57] thereby increasing the cholesterol content in the fluid phase.

(iv) The mobility of PGPE-Alexa647 is substantially higher than the mobility of DHPE-Bodipy in ordered or obstructed matrices. In the liquid ordered phase of a ternary system, a mobility ratio of $R = 2.3$ was obtained. Moreover, when we artificially increased the obstacle density in a fluid supported lipid bilayer by immobilizing biotin-DOPE in the proximal bilayer leaflet on avidin, the ratio dramatically increased to $R = 51.1$. Deverall et al. described the effect of random obstacles on lipid mobility by extending the free area theory[56] and reported nonlinear dependence on the tracer size.[58] Essentially, large tracers are more easily stuck between obstacles than small tracers. This effect appears directly relatable to the plasma membrane, where immobilized lipids or acylated proteins on the cytosolic leaflet provide a similar obstructed matrix for tracers located at the exoplasmic leaflet.

Conclusions

In summary, we have found that the oxidized phospholipid PGPC and its fluorescent analogue PGPE-Alexa647 move with increased mobility compared to conventional phospholipids. The lysolipid-like character enables the probe to enter ordered environments, thereby providing a means for spreading rapidly and homogeneously over complex matrices like the cellular plasma membrane. Mobility is not only determined by the fluidity of the matrix, but also by immobile obstacles or by the localization of the probe along the bilayer normal, which can be influenced by the cholesterol concentration.

(57) London, M.; London, E. Ceramide selectively displaces cholesterol from ordered lipid domains (rafts) - Implications for lipid raft structure and function. *J. Biol. Chem.* **2004**, *279*(11), 9997–10004.

(58) Deverall, M. A.; Gindl, E.; Sinner, E. K.; Besir, H.; Ruehe, J.; Saxton, M. J.; Naumann, C. A. Membrane lateral mobility obstructed by polymer-tethered lipids studied at the single molecule level. *Biophys. J.* **2005**, *88*(3), 1875–86.